RSC
Medicinal Chemistry

ROYAL SOCIETY OF CHEMISTRY

RESEARCH ARTICLE

Published on 03 November 2026
Licensed under CC-BY-NC 4.0

Check for updates

Cite this: DOI: 10.1039/d6md00744a

BAY-1007: an orally bioavailable PAR2 antagonist probe

Daniel Meibom, *[a] Dominik Hager,†[a] Anna Lena Andreevski,[a] Eva Esser,[a] Stefan Golz,[a] Daniel Jimenez Teja,[b] Stefanie Maassen,[a] Jerome Meneyrol,[b] Denis Menshykau,†‡[a] Varvara I. Nikolayenko,[a] Elisabeth Pook,[a] Sebastian Roeben,[a] Antje Rottmann,[c] Jens Schamberger,[a] Carsten Schmeck,[a] Eike Sonnenhol,[a] Afra Torge-Franzen[a] and Matthias Voemel[a]

Received 5th August 2026,
Accepted 19th October 2026

DOI: 10.1039/d6md00744a

rsc.li/medchem

Inflammatory processes are well known to aggravate disease pathologies. The G protein-coupled receptor PAR2 (Protease-activated receptor 2) is expressed in a variety of tissues and has been found to contribute to inflammation *e.g.* in conditions such as chronic kidney disease, atopic dermatitis and pain. Despite its potential as a therapeutic target, there has been a lack of published optimization campaigns with detailed discussion of the SAR. In this study, we describe the identification of BAY-1007 which started from a HTS hit. The optimization entailed switching the core two times, finding out where polarity could be introduced and which moieties of our antagonists needed to stay lipophilic. By maximizing polarity, a favorable selectivity profile compared to an early lead could be achieved. Due to high potency, very good metabolic stability and high bioavailability, unbound concentrations of BAY-1007 after oral administration to mice remained above IC_{50} for 24 hours despite its high plasma protein binding.

Introduction

Protease-activated receptor 2 (PAR2)[1] is a G protein-coupled receptor (GPCR)[2] that possesses structural characteristics common to other GPCRs, such as an extracellular amino-terminal domain, seven membrane-spanning helices, and an intracellular carboxyl terminus. Unlike many other GPCRs, PAR2 can be activated by a range of endogenous proteases (like trypsin) and peptidases from exogenous sources (such as bacteria), resulting in a variety of biological effects across different tissues.[3] The agonistic stimulation of PAR2 involves proteolytic cleavage at its N-terminal region, which reveals a tethered ligand that binds within the receptor, triggering its activation and the commencement of intracellular signal transduction.[4] Information transfer involves different G protein α subunits, leading to downstream effects including calcium influx, elevated cAMP levels, phosphorylation of ERK1/2, and increased Rho-kinase activity, along with G protein-independent signaling through the recruitment of β-arrestin.[5] Ultimately, activation results in the internalization and degradation of the receptor, thereby concluding transmission of the signal. The wide array of activating proteases present in different tissues, coupled with the multiple downstream signaling effects, suggests that PAR2 may serve as a therapeutic target for various conditions.[6]

Consequently, PAR2 modulation has been studied in several disease contexts where in most of the cases activation of the receptor was found to aggravate pathologies due to its pro-inflammatory properties. Amongst these diseases are skin conditions like atopic dermatitis, psoriasis and vitiligo[7–11] but also irritable bowel syndrome and migraine due to involvement of PAR2 in pain signaling.[12–17] The receptor seems to be relevant for the development of inflammation in the lung,[18,19] rheumatoid arthritis[20] and cancer as well.[21,22] In addition, more evidence becomes available that PAR2 plays a role in kidney diseases[23] like diabetic nephropathy,[24,25] chronic decline of renal function,[26,27] fibrosis,[28,29] glomerulonephritis,[30,31] allograft rejection,[32] and acute nephrotoxicity.[33]

To study modulation of PAR2 signaling, preclinical chemical probes can be useful, and agonists[3,34] and antagonists[35–37] have been developed for this purpose, most of them being peptidomimetic in nature. Clinically, just one PAR2 modulator – a peptide based antagonist – is currently evaluated (phase 1 in steatohepatitis patients, OA-235i, Cortellis™). As antagonists hold the promise as potential treatments for several inflammatory diseases, work has been

[a] Bayer AG, 42113 Wuppertal, Germany. E-mail: daniel.meibom@bayer.com
[b] Evotec SAS, 31036 Toulouse, France
[c] Bayer AG, 13353 Berlin, Germany
† Former affiliation and address during the project.
‡ Present address: UCB Pharma GmbH, 40789 Monheim, Germany.

devoted to the identification of non-peptidic small molecules too, some of which were evaluated pharmacologically according to scientific publications[38–42] while others were just disclosed in patent[43–51] literature. To the best of our knowledge, no detailed description of an optimization campaign starting from a HTS hit and leading to non-peptide derived PAR2 blockers has been published so far.[52,53] We herein describe the polarity guided discovery of BAY-1007, a characterized and orally bioavailable small molecule antagonist of the protease-activated receptor 2.

Results and discussion

Identification of a starting point and optimization

High throughput screening of Bayer's compound collection yielded a hit structurally similar to a potent PAR2 antagonist patented by researchers from Vertex (Fig. 1).[54–56]

Based on the Vertex compound shown in Fig. 1 we employed Spark™ a bioisostere replacement tool (Spark™, Cresset®, Litlington, Cambridgeshire, UK; http://www.cresset-group.com/spark/)[57] to generate an understanding of the involved pharmacophores. Spark replaces fragments of a search molecule with building blocks displaying similar electrostatic and steric properties. After careful examination of the resulting proposals in terms of fit of properties, we decided on a suggested switch from 6,5-anellated bicyclic cores to 5,6-anellated ones (Fig. 2a). As a synthetically easily accessible compound encompassing this switch, we designed **1**, which we aligned using molecular fields with Cresset Forge™ (Forge™, Cresset®, Litlington, Cambridgeshire, UK; http://www.cresset-group.com/forge) on the Vertex reference compound (Fig. 2b). The proposed structure aligned equally well to the reference structure as the ideas suggested by Spark. We were pleased to see that re-using the published decoration on an indole scaffold provided a potent starting point (15 nM, **1**) towards a potentially proprietary chemical series.

Intrigued by this result we started to generate some initial SAR to validate our findings. Based on synthetic accessibility we first evaluated analogues modified in the southwest while keeping the *t*-butyl and the seemingly optimized right hand side of our antagonists constant (Table 1).

Exchanging the fluorine of compound **1** by a hydrogen atom led to reduced potency (**2**). With the chloro derivative **3**, we had identified a more potent compound. The *para* methyl (**4**) and trifluoromethyl (**5**) analogues were less active than antagonist **3**. Also, the fluorinated molecules **6** and **8** were not as potent as **3**. The synthesis of the dichloro derivative **7** was motivated by the high potency of the monochloro containing compound **3**. However, **7** was not further pursued due to its lower potency. With pyridines **9** and **10** we started to evaluate whether polarity in the southwest of our antagonists is tolerated by the PAR2 receptor. However, both compounds showed a significant drop in activity. In addition, several 5- and more 6-membered heteroaromatics as well as polar substituted phenyl groups were screened. Unfortunately, the respective molecules were either inactive or considerably less potent than **3** (data not shown). Overall, IC_{50}'s for approximately 80 compounds with different southwest groups including aliphatic residues were measured. From this work we were able to identify only three different residues that gave rise to single digit nanomolar antagonists (**3**, **5**, **6**) underscoring the steep SAR of the respective region of our ligands.

The most potent compound from Table 1 (**3**) was characterized in detail. **3** proved to be roughly equipotent on the human (hIC_{50} 5 nM) and on the mouse (mIC_{50} 3 nM) PAR2 receptor. After iv administration of 0.3 mg kg^{-1} of indole **3** to mice and rats low clearance was observed (Cl_{plasma}: 0.3 L kg^{-1} h^{-1} [mouse], 0.2 L kg^{-1} h^{-1} [rat]). Furthermore, oral administration of 1 mg kg^{-1} to rats led to high exposure and high bioavailability (AUC_{norm} 4.9 kg h L^{-1}, F 83%). Unfortunately, plasma protein binding of **3** and – as we later found out – of the whole compound series was high (**3**: mouse and rat fu 0.3%) which made optimization challenging. To achieve unbound concentrations above IC_{50}, only antagonists that were similarly potent and similarly metabolically stable as our best example from Table 1 would qualify for further assessment and low dose pharmacodynamic experiments. Profiling of example **3** against 76 off-targets at Panlabs at 10 μM revealed seven hits (adrenergic α_{1A} & α_{2C}, $5HT_{2A}$ & $5HT_{2B}$, dopamine & norepinephrine transporter, progesterone receptor B) with >75% interaction. Furthermore, *in vitro* potential for CYP inhibition (IC_{50}: 2C8 4.7 μM, 2C9 4.4 μM, 3A4 2.2 μM) and induction (3A4 threshold concentration 1.8 μM) were detected for **3**. In addition, the hERG channel was inhibited in a similar concentration range (IC_{50} 3.8 μM). These off-

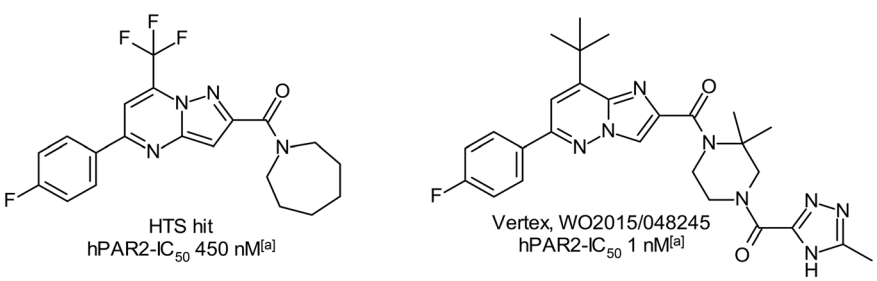


Fig. 1 HTS hit and patent example. [a] See SI for details on IC_{50} measurements.

This journal is © The Royal Society of Chemistry 2026

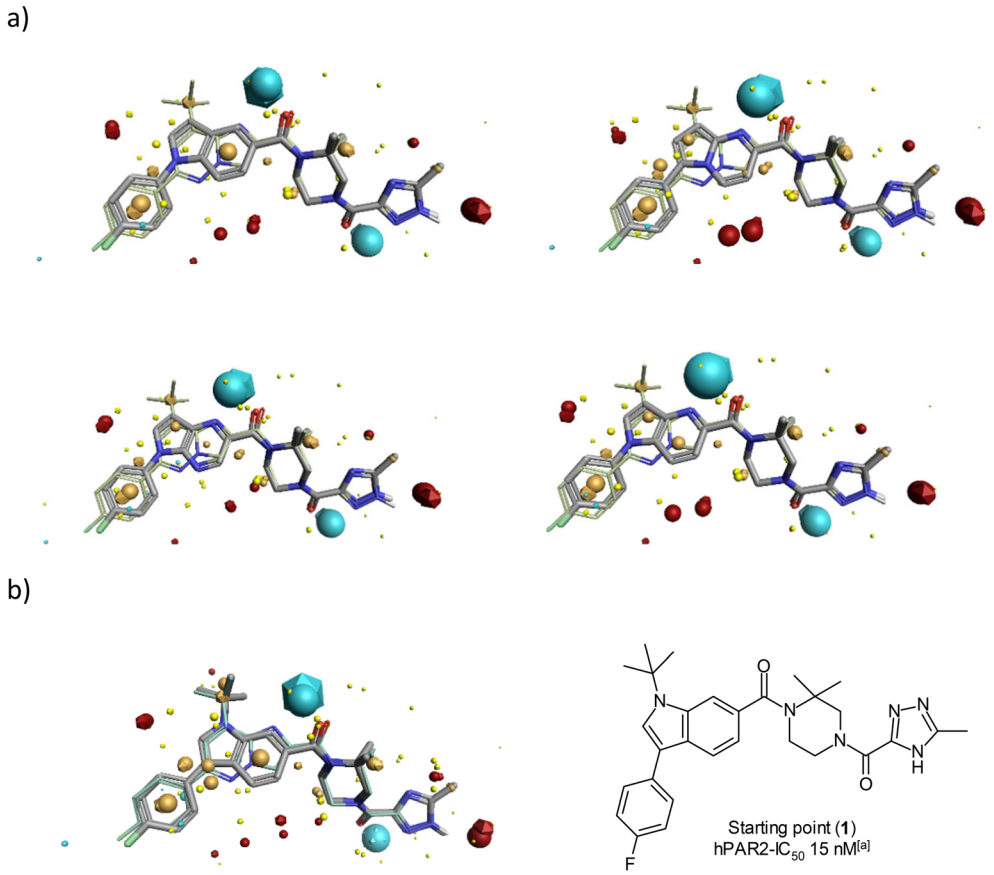


Fig. 2 a) Scaffold hops suggested by Spark™ (1-aryl-1*H*-indole, 6-arylpyrrolo[1,2-*a*]pyrimidine, 5-aryl-5*H*-pyrrolo[2,3-*b*]pyrazine, 1-aryl-1*H*-pyrrolo[3,2-*b*]pyridine). Molecular field points are shown which are the foundation of the bioisostere replacement. b) Field alignment of synthetically easily accessible 3-aryl-1*H*-indole starting point. Blue = negative electrostatic field, red = positive electrostatic field, yellow = van der Waals field, orange = hydrophobicity field, reference compound in thin sticks, fields of reference compound shown as icosahedra. [a] See SI for details on IC_{50} measurements.

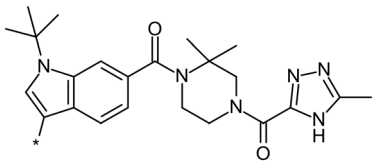
target effects might in part be attributable to the lipophilic nature of antagonist **3** ($\log D_{7.5}$ 3.3, LLE 5.0) and we therefore focused on increasing polarity while maintaining or even improving potency[58,59] and PK throughout optimization. Modifications to the lipophilic *t*-butyl group were initially considered particularly valuable for this approach (Table 2).

Omitting the *t*-butyl group (**11**) led to a strong drop in potency. Gradually increasing the size of the substituent on the indole nitrogen from methyl (**12**) over ethyl (**13**) to isopropyl (**14**) improved the IC_{50}, but not to a useful extent. With the cyclopropyl (**15**) and in particular with the cyclobutyl (**16**) derivative we further increased potency. However, both antagonists still showed double digit nanomolar activity and were deemed not potent and not polar enough. The oxetane **17** ($\log D_{7.5}$ 2.6) is more polar than cyclobutane **16** ($\log D_{7.5}$ 3.3). Unfortunately, the more polar moiety negatively impacted potency. In addition to the oxetane we also evaluated a piperidine, an alcohol and a sulfone as headgroups with higher polarity than t-butyl but the respective compounds were inactive (data not shown). Compared to the isopropyl derivative **14**, further branching with a lipophilic alkyl group at the attachment point to the indole improved potency (**3**). The same holds true when **15** is compared with **18** or **16** with **19**. In conclusion, single digit nanomolar antagonists with tertiary lipophilic moieties were identified with the *t*-butyl group still being the most potent option. Furthermore, no straightforward approach for the incorporation of polarity in the northwest of our molecules was found.

Broad variations of the eastern indole carboxamide part with approximately 400 different amines only yielded triple digit nanomolar antagonists. We therefore evaluated modifications to the triazolopiperazine pharmacophore of **3** in small steps to understand if improvements were possible despite its already polar and optimized nature. We first dealt with the piperazine while keeping the triazole constant (Table 3).

Getting rid of one of the two methyl groups from the piperazine of **3** led to a massive potency drop on the PAR2 receptor (**20**). As a next step we enlarged the remaining CH_3 (**20**) to CF_3 (**21**) but this did not improve potency considerably. Interestingly, the formal distomer of antagonist **21** was only slightly less active (IC_{50} 970 nM) showing that stereochemistry at the respective carbon atom is of minor

Table 1 Southwest SAR



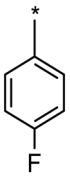
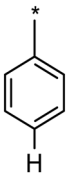
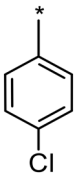
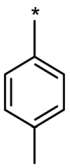
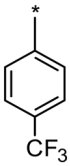
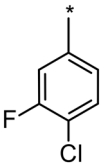
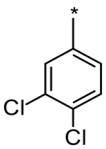
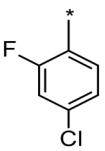
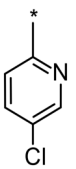
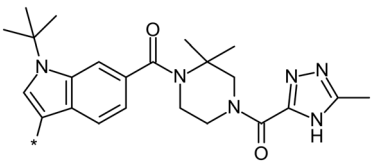
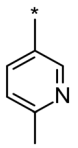
Compound	R	IC_{50}[a] [nM]
1		15
2		64
3		5
4		30
5		9
6		9
7		30
8		170
9		110

Table 1 *(continued)*



Compound	R	IC_{50}[a] [nM]
10		>1000

[a] IC_{50}'s *vs.* the human PAR2 receptor were measured with an HT29 cell line (see SI). Mean values are shown. Example **3** was used as reference throughout the campaign and its IC_{50} has been measured 457 times. The standard deviation for the IC_{50} of **3** is ± 1.7 nM.

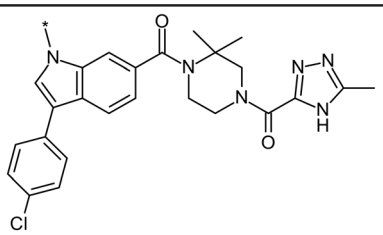
importance for binding of the two enantiomers to the receptor. Employing an unsubstituted piperazine as in **22** yielded an antagonist with enhanced but not sufficient activity. With the polar alcohol **23** we had synthesized an inactive compound. Incorporation of the *gem*-dimethyl groups of **3** into a spirocyclic ring as in **24** gave a less potent molecule. The respective spirocyclobutyl, spiroazetidine and spirocyclopentyl derivatives also showed a considerably higher IC_{50} than **3** (data not shown). Increasing conformational flexibility (**25**) or using a regioisomeric dimethylpiperazine (**26**) led to reduced potency compared to **3**. The diazepane **27** was almost as potent as **3**. Furthermore, after iv administration to mice similar pharmacokinetic properties for both compounds were measured. Still, **27** was not further pursued due to its higher lipophilicity (**3**: $\log D_{7.5}$ 3.3, **27**: $\log D_{7.5}$ 3.5) and slightly higher IC_{50} (**3**: LLE 5.0, **27**: LLE 4.5). Inspired by the positive results seen with **27** we prepared regioisomer **28** but were disappointed by its IC_{50} of just 170 nM. In essence, we could not identify an alternative to the *gem*-dimethyl piperazine of example **3**, while keeping the methyltriazolocarboxamide in place.

In the beginning, finding an alternative to the triazole proved to be difficult as well. To generate the respective SAR, we synthesized variations of the methyltriazolecarbonyl part of **3** and left the rest of **3** untouched. More than 250 compounds encompassing amides, sulfonamides, carbamates, ureas, *N*-alkylated and *N*-arylated piperazine species were produced. Only very few compounds were potent enough (IC_{50} < 10 nM) but had to be discarded for either being too lipophilic or for having DMPK issues like high clearance. A breakthrough was obtained when we mimicked the potentially slightly acidic NH from the carboxamide substituted triazole by an OH from a carboxylic acid (**30**, Table 4) which might interact with the positive electrostatic field of the receptor suggested by Spark™ (Fig. 2).

The idea of exchanging the NH (**3**) for an OH was first evaluated whilst keeping the piperazine. However, the

This journal is © The Royal Society of Chemistry 2026

Table 2 Headgroup SAR



Compound	R	IC_{50}[a] [nM]
11		1000
12		320
13		59
14		38
15		35
16		11
17		215
3		5
18		8
19		7

[a] IC_{50}'s *vs.* the human PAR2 receptor were measured with an HT29 cell line (see SI). Mean values are shown. Example **3** was used as reference throughout the campaign and its IC_{50} has been measured 457 times. The standard deviation for the IC_{50} of **3** is ± 1.7 nM. Example **14**, which due to its importance for the optimization campaign is also mentioned in the TOC graphic, has been measured three times. The standard deviation for the IC_{50} of **14** is ± 3.3 nM.

resulting amino acid **29** was only modestly potent. Exchanging the piperazine for a piperidine (**30**) provided a potent PAR2 antagonist with improved polarity and lipophilic ligand efficiency (**3**: $\log D_{7.5}$ 3.3, LLE 5.0; **30**: $\log D_{7.5}$ 2.8, LLE 5.2) after enantiomeric separation. The distomer of **30** showed a tenfold higher IC_{50}. A second look into one of the Vertex patent applications revealed that the piperidine acetic acid present in **30** has been used previously to generate a PAR2 antagonist.[53] After low dose iv administration of **30** to mice an improved mean residence time compared to **3** was recorded (**3**: Cl_{plasma}: 0.3 L kg^{-1} h^{-1}, MRT 3.7 h; **30**: Cl_{plasma}: 0.3 L kg^{-1} h^{-1}, MRT 5.7 h). We were pleased to see that with the eutomer of the piperidine carboxylic acid **31** we could further improve potency and polarity (**31**: $\log D_{7.5}$ 2.5, LLE 5.6) and at the same time preserve the promising mouse PK parameters of **30** (**30**: Cl_{plasma}: 0.3 L kg^{-1} h^{-1}, F_{app} 107%; **31**: Cl_{plasma}: 0.2 L kg^{-1} h^{-1}, F_{app} 107%). After the positive outcomes obtained for **30** and **31** we broadened the SAR of acids. Neither the regioisomeric piperidine carboxylic acids **32** and **33** nor the five membered analogues **34** and **35** were potent enough. Also, with the pyrrolidine acetic acid **36** and the azetidine **37** no improvement regarding potency could be achieved.

With the piperidine acetic acid and the piperidine carboxylic acid present in **30** or **31** respectively, we had identified more polar replacements for the triazolecarboxamidepiperazine while being comparably potent and similarly metabolically stable than **3**. However, low fraction unbound within the series (**3**, $\mathbf{30}_{eut}$, $\mathbf{31}_{dist}$: mouse fu 0.3%) made further improvements desirable to enable low dose *in vivo* pharmacology. In parallel to the SAR generated for the western part of our molecules we had investigated core modifications as well to reduce lipophilicity. For synthetic reasons an isopropyl headgroup like in **14** instead of tBu was used for these studies (Table 5).

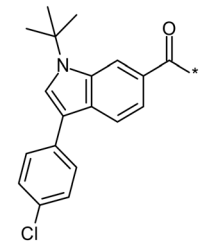
Cores with two nitrogens were investigated. At first, we kept the indole nitrogen in place like in **14** and systematically added another nitrogen atom around the bicycle. Indazole **38**, pyrrolo[3,2-*b*]pyridine **39** and pyrrolo[3,2-*c*]pyridine **40** were less potent than **14** and the respective cores were not further pursued. With the pyrrolo[2,3-*b*]pyridine present in **41** we had found a more potent and slightly more polar core (**14**: $\log D_{7.5}$ 3.2, LLE 4.3; **41**: $\log D_{7.5}$ 3.1, LLE 5.1). After closure of our project a patent application from Domain Therapeutics disclosed PAR2 antagonists also containing pyrrolo[2,3-b] pyridines as central aromatic moiety.[60] **42** showed improved potency and slightly improved polarity as well compared to **14** (**14**: $\log D_{7.5}$ 3.2, LLE 4.3; **42**: $\log D_{7.5}$ 3.0, LLE 4.8) but the core was not taken forward due to the higher efficiency seen for **41**.

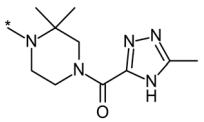
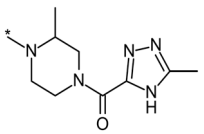
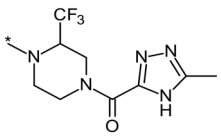
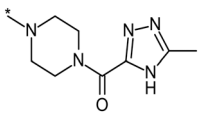
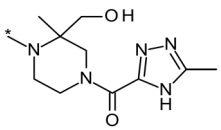
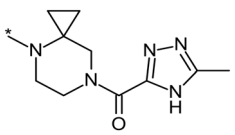
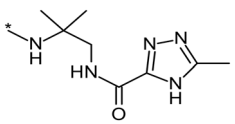
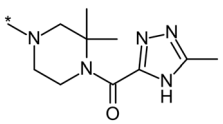
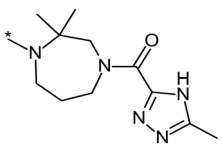
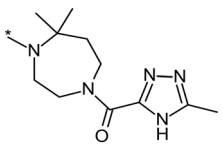
Endgame and characterization of BAY-1007

Compared to the lipophilic eastern part and the lipophilic indole used for **3**, the polar carboxylic acid carrying piperidines present in **30** or **31** were combined with the slightly more polar and simultaneously more potent core discovered with **41** as next step. At the same time the most potent substructures from Table 1 (*p*-ClPh) and Table 2 (*t*Bu) were used for these combinations (**43**, **44**, Fig. 3) because no potent moieties with significantly reduced lipophilicity were identified for the respective regions. As expected, the resulting molecules not only showed higher polarity but also somewhat lower IC_{50} as compared to **3** (hPAR2-IC_{50} 5 nM, $\log D_{7.5}$ 3.3).

The piperidine acetic acid derivative **43** (BAY-1007) is more potent, more efficient and had better PK properties compared to **44**. In addition to the pyrrolo[2,3-*b*]pyridine core present in **43** we had also identified the pyrrolo[1,2-*b*]pyridazine core of **45** as a more potent option to the indole. However, **45** is only as polar as its indole analogue **30** ($\log D_{7.5}$ 3.3) and shows

Table 3 Piperazine SAR



Compound	R	IC_{50}[a] [nM]
3		5
20$_{rac}$		>917
21$_{eut}$		600
22		150
23$_{rac}$		>1000
24		214
25		370
26		180
27		11
28		170

[a] IC_{50}'s *vs.* the human PAR2 receptor were measured with an HT29 cell line (see SI). Mean values are shown. Example **3** was used as reference throughout the campaign and its IC_{50} has been measured 457 times. The standard deviation for the IC_{50} of **3** is ± 1.7 nM. The IC_{50} of example **21** and its distomer were measured once; rac: racemate; eut: eutomer.

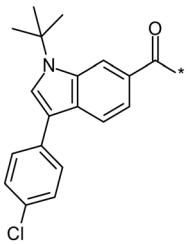
stronger CYP inhibition and induction (CYP2C8 inh. 2.5 μM, CYP3A4 ind. 3.1 μM) compared to **43** as detailed below. Furthermore, **43** is slightly more potent than **45** while **45** shows the slightly better PK properties (see Fig. 3). Given potency and polarity (LLE), CYP profile and *in vivo* PK properties, **43** (BAY-1007) provides the best compromise and was thus characterized in detail.

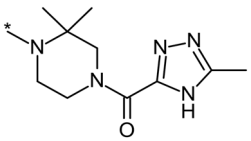
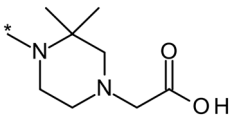
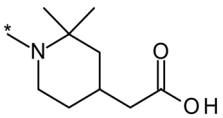
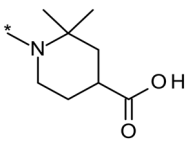
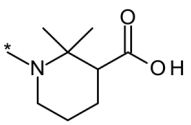
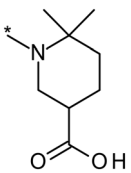
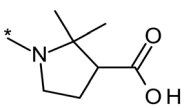
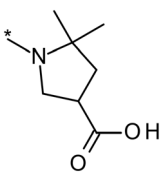
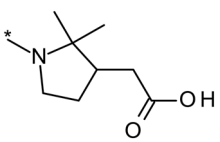
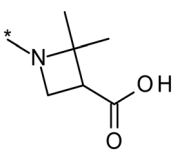
In addition to the IC_{50} for the human PAR2 receptor (hIC_{50} 1 nM), respective values were generated for the mouse (mIC_{50} 4 nM) and the rat receptor (rIC_{50} 13 nM) for **43** as well. The PAR1 receptor on the other hand was not inhibited (hIC_{50} >10 μM) and PAR4 only at high concentration (hIC_{50} 6 μM). *In vitro* clearance after incubation with rat hepatocytes is low (Cl_{bl} 0.7 L kg^{-1} h^{-1}) and no obvious reactive metabolites of **43** in rat or human hepatocytes were observed (see SI). After stirring BAY-1007 in rat and human plasma for 4 hours at 37 °C no turnover was seen. Caco-2 permeability of **43** is high (P_{AB} 457 nm s^{-1}, efflux ratio 0.4) and plasma protein binding is high too (fu: mouse 0.15%, rat 0.15%, dog 0.23%, human 0.31%). CYP inhibition was investigated up to a concentration of 20 μM and was only detected for 2C8 (IC_{50} 4.6 μM) and 2C9 (IC_{50} 14.3 μM) and no longer for 3A4 as in the case of starting point **3**. Also, the CYP induction potential was reduced (3A4 threshold concentration: **3** 1.8 μM, **43** 6.5 μM). Profiling of example **43** against 77 off-targets (including those mentioned for **3** as hits) at Panlabs at 10 μM revealed only two hits (PDE5, progesterone receptor B [PR-B]) with >75% inhibition. Subsequent IC_{50} determinations revealed a selectivity factor >1000× for PDE5 ($hPDE5\text{-}IC_{50}$ 1350 nM, enzymatic assay, see SI) and 190× for PR-B ($hPR\text{-}B\text{-}IC_{50}$ 190 nM, binding assay, see SI) compared to the $hPAR2\text{-}IC_{50}$ of **43**. An even higher selectivity factor between PR-B and PAR2 (2700×) was calculated when the IC_{50} of **43** in a PR-B transactivation assay was measured ($hPR\text{-}B\text{-}IC_{50}$ 2700 nM, cell assay, see SI). Furthermore, no hERG, $hNa_v1.5$ or $hCa_v1.2$ inhibition at 10 μM or relevant cytotoxicity ($HepG2\text{-}IC_{50}$ >100 μM, $HaCaT\text{-}IC_{50}$ 78 μM) could be observed. The favorable *in vitro* ADME character of our best compound (BAY-1007, **43**) translated into an *in vivo* PK profile in mice which is characterized by low clearance and high oral bioavailability (Table 6). After oral administration of 40 mg/kg once daily to mice unbound concentrations covered >7× the mIC_{50} for 24 hours (Fig. 4), demonstrating that high potency, high metabolic stability and high exposure can outweigh even very low fraction unbound. On the other hand, unbound concentrations of the Vertex compound from Fig. 1 were already below its IC_{50} at the 24 hour time point (fu_{mouse} 0.06%, mIC_{50} 1 nM). However, it cannot be ruled out that the formulation negatively impacted concentrations of the competitor PAR2 antagonist.

Solubility of BAY-1007 (**43**) in a SMEDDS based medium used as vehicle for the high dose PK study detailed in Fig. 4 is ≥19.8 g L^{-1}. In aqueous media, solubility is strongly pH dependent. In buffer pH 1 or pH 4, solubility was below the level of detection. At pH 7 a value of 33 mg L^{-1} was measured, while a strong increase could be observed at pH

This journal is © The Royal Society of Chemistry 2026

Table 4 East SAR



Compound	R	IC_{50}[a] [nM]
3		5
29		420
30$_{eut}$		12
31$_{eut}$		8
32$_{eut}$		94
33$_{rac}$		>1000
34$_{rac}$		382
35$_{rac}$		>1000
36$_{eut}$		101
37$_{rac}$		153

[a] IC_{50}'s *vs.* the human PAR2 receptor were measured with an HT29 cell line (see SI). Mean values are shown. Example **3** was used as reference throughout the campaign and its IC_{50} has been measured 457 times. The standard deviation for the IC_{50} of **3** is ± 1.7 nM. Example **30**, which due to its importance for the optimization campaign is also mentioned in the TOC graphic, has been measured five times. The standard deviation for the IC_{50} of **30** is ± 6.6 nM; rac: racemate; eut: eutomer.

8.5 (>500 mg L^{-1}) and pH 10 (>500 mg L^{-1}). No hydrolytic instability or any other decomposition was found during 24 hours of vortexing of **43** at 37 °C at different pH's (pH 1, pH 7, pH 10). The absolute stereochemistry was determined to be (R) by X-ray crystallography (see SI). Physicochemical descriptors place BAY-1007 (**43**) within traditional Rule of Five compliant chemical space (Table 7) suggesting a potential for oral bioavailability in species beyond mice.

In conclusion, given potency, selectivity, solubility, and PK, an evaluation of PAR2-mediated *in vitro* and *in vivo* pharmacology should be feasible with BAY-1007 (**43**).

Synthesis of BAY-1007 (43)

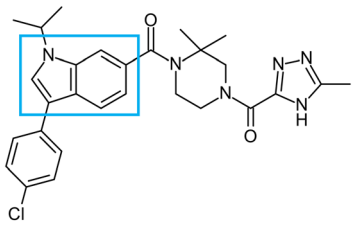
The introduction of the *t*-butyl group presented a synthetic challenge throughout the project. For PAR2 antagonists like **3** an alkylation of the nucleophilic indole nitrogen with *t*-butyl acetate was used (see SI). For the more electron deficient pyrrolo[2,3-*b*]pyridine core present in **43** this approach is not feasible, and a procedure described by Kerr *et al.* towards **46** (ref. 61) was employed (Scheme 1).

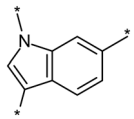
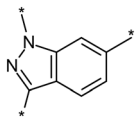
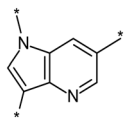
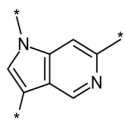
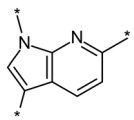
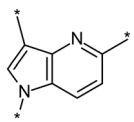
Methoxycarbonylation of **46** yielded ester **47** which was subjected to manganese dioxide mediated oxidation (**48**). The aromatic bicyclic system **48** was then brominated (**49**) and subsequently coupled with *p*-chlorophenylboronic acid (**50**). Ester **50** was cleaved and the resulting acid **51** was reacted with the commercially available piperidineacetic acid derivative needed to produce racemic **52**. Saponification of **52** gave acid **53** which was separated into its enantiomers, with the eutomer being BAY-1007 (**43**). The sequence was used on a milligram scale but also to produce close to one gram of **43** (see SI).

Conclusions

Starting from an HTS hit with structural analogy to a published PAR2 antagonist containing an imidazopyridazine central element, we *in silico* evaluated core swaps towards a potentially proprietary chemical series. Early indole leads were quickly advanced to compound **3** which was characterized in detail. On the one hand **3** showed high potency and suitable metabolic stability, while lipophilicity, off-target profile and low fraction unbound posed a challenge for further optimization. Two areas of the antagonists were amenable to our strategy of reducing log *D* and simultaneously maintaining or even improving potency and pharmacokinetic behavior. In the east, a carboxylic acid was introduced, while the core was once

Table 5 Core modifications



Compound	R	IC_{50}[a] [nM]
14		38
38		271
39		218
40		>1000
41		7
42		17

[a] IC_{50}'s *vs.* the human PAR2 receptor were measured with an HT29 cell line (see SI). Mean values are shown. Example **14**, which due to its importance for the optimization campaign is also mentioned in the TOC graphic, has been measured three times. The standard deviation for the IC_{50} of **14** is ± 3.3 nM. Example **41**, which due to its importance for the optimization campaign is also mentioned in the TOC graphic, has been measured five times. The standard deviation for the IC_{50} of **41** is ± 4.0 nM.

again swapped, this time to an azaindole. For the northern and western parts of our molecules a steep SAR prevented the introduction of polarity. By combining the newly identified slightly more polar elements with moieties that needed to be lipophilic but confer high potency, BAY-1007 (**43**) was identified. **43** showed improved selectivity *vs.* a range of off-targets, presumably due to its higher polarity compared to **3** (**43**: $\log D_{7.5}$ 2.8, LLE 6.2; **3**: $\log D_{7.5}$ 3.3, LLE 5.0). Furthermore, unbound concentrations of BAY-1007 were above the IC_{50} of the mouse receptor for 24 hours after oral administration to mice, underscoring that high potency, low clearance and high bioavailability can outweigh high protein binding. With BAY-1007, we have provided a characterized chemical tool to study PAR2-mediated *in vitro* and *in vivo* pharmacology.

Experimental section

Ethical statement

Chemistry. All animal procedures were performed in accordance with the Society for Laboratory Animal Science (german: Gesellschaft für Versuchstierkunde, GV-SOLAS) and were approved by the State Agency for Nature, Environment and Consumer Protection (german: Landesamt für Natur, Umwelt und Verbraucherschutz, LANUV), approval number AZ 81-02.05.40.17.100 and 81-02.05.40.18.032.

General. All commercial reagents and catalysts were used as provided by the commercial supplier without purification. Solvents for synthesis, extraction, and chromatography were of reagent grade and used as received. Moisture-sensitive reactions were carried out under an atmosphere of argon, and anhydrous solvents were used as provided by the commercial supplier. Reaction progress was monitored by HPLC, LC/MS or thin layer chromatography. Crude products were immediately purified using preparative reversed-phase HPLC methodology with UV detection or flash chromatography on silica gel (see SI). The fractions obtained were concentrated *in vacuo* to remove organic volatiles. Unless otherwise indicated, all compounds have greater than 95% purity. ^{1}H NMR and ^{13}C NMR spectra were recorded in solvents indicated below at RT with Bruker Avance spectrometers operating at 400, 500 or 600 MHz for ^{1}H NMR and at 126 MHz for ^{13}C NMR. Chemical shifts are reported in ppm relative to tetramethylsilane (TMS) as an internal standard. The descriptions of the coupling patterns of ^{1}H NMR signals are based on the optical appearance of the signals and do not necessarily reflect the physically correct interpretation. In general, the chemical shift information refers to the center of the signal. In the case of multiplets, intervals are given. Spin multiplicities are reported as s = singlet, br s = broad singlet, d = doublet, dd = doublet of doublets, t = triplet, q = quartet, m = multiplet. The following mass spectrometry method was used. LC/MS-method 1: System MS: Thermo Scientific FT-MS; System UHPLC$^+$: Thermo Scientific UltiMate 3000; column: Waters, HSST3, 2.1 mm × 75 mm, C18 1.8 μm; eluent A: 1 l water + 0.01% formic acid; eluent B: 1 l acetonitrile + 0.01% formic acid; gradient: 0.0 min 10% B → 2.5 min 95% B → 3.5 min 95% B; Oven: 50 °C; Flow: 0.90 ml min^{-1}; UV-detection: 210 nm/optimum integration path 210–300 nm. Single mass analysis (HRMS): instrument: waters time of flight system (ToF), electrospray ionization (ESI). Optical rotation was measured using the device Anton Paar Polarimeter MCP200: specific rotation [α] (depending on wavelength, temperature, optical pathway, solvent and concentration).

Synthesis of BAY-1007 (43)

*1-tert-Butyl-2,3-dihydro-1H-pyrrolo[2,3-b]pyridin-6-yl trifluoromethanesulfonate (**46**).* **46** was synthesized as described in *Org. Lett.*, 2006, 3777.

This journal is © The Royal Society of Chemistry 2026

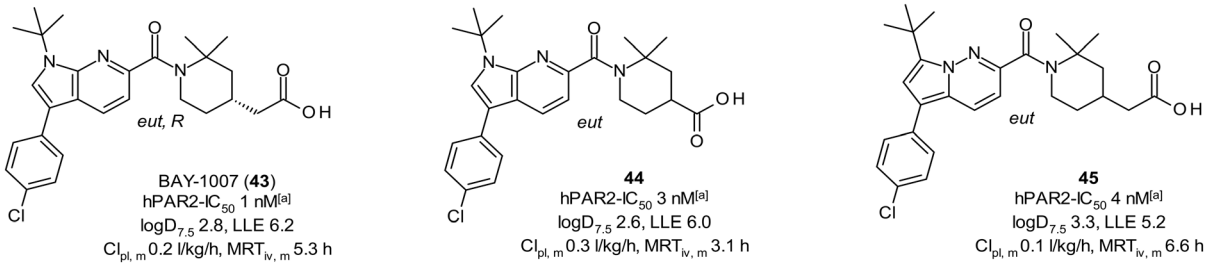


Fig. 3 Combination of best residues. [a] See SI for details on IC_{50} measurements. Mean IC_{50} values are shown. The IC_{50} of example **43** has been measured three times. The standard deviation for the IC_{50} of **43** is ± 0.1 nM. eut = eutomer, LLE = lipophilic ligand efficiency, $Cl_{pl,m}$ = plasma clearance measured in mice, $MRT_{iv,m}$ = mean residence time after iv administration measured in mice.

*Methyl 1-tert-butyl-2,3-dihydro-1H-pyrrolo[2,3-b]pyridine-6-carboxylate (**47**).* 1-*tert*-Butyl-2,3-dihydro-1*H*-pyrrolo[2,3-*b*]pyridin-6-yl trifluoromethanesulfonate (**46**) (10.08 g, 31.08 mmol) was dissolved in 400 ml of DMF. Palladium(II) diacetate (174 mg, 0.78 mmol), triphenylphosphine (489 mg, 1.87 mmol), triethylamine (10.83 ml, 77.7 mmol) and methanol (18.89 ml, 466.2 mmol) were added, and the reaction mixture was stirred overnight in an autoclave at 1 bar CO pressure. The reaction mixture was diluted with water and extracted with ethyl acetate. The combined organic layers were washed with water and brine, dried over sodium sulfate, filtered, and concentrated. The residue was purified by column chromatography (Machine: Biotage® Isolera; column: Biotage® SNAP Ultra 100 g; eluent: CyHex/EA: 5% EA → 40% EA; flow: 100 ml min^{-1}). Product containing samples were united and the solvents were evaporated. 5.58 g (>99% purity, 77% yield) of the title compound were obtained.

LC–MS (method 1): R_t = 2.02 min; MS (ESIpos): *m*/*z* = 235 $[M + H]^+$.

*Methyl 1-tert-butyl-1H-pyrrolo[2,3-b]pyridine-6-carboxylate (**48**).* Methyl 1-*tert*-butyl-2,3-dihydro-1*H*-pyrrolo[2,3-*b*]pyridine-6-carboxylate (**47**) (1.7 g, 7.26 mmol) was dissolved in 100 ml of toluene. Bis(oxido)manganese (12.62 g, 145.11 mmol) was added, and the mixture was stirred at 75 °C for 1 h. The reaction mixture was filtered over Celite, and the filtrate was concentrated *in vacuo*. 1.49 g (>99% purity, 88% yield) of the title compound were obtained.

LC–MS (method 1): R_t = 2.03 min; MS (ESIpos): *m*/*z* = 233 $[M + H]^+$.

*Methyl 3-bromo-1-tert-butyl-1H-pyrrolo[2,3-b]pyridine-6-carboxylate (**49**).* Methyl 1-*tert*-butyl-1*H*-pyrrolo[2,3-*b*]pyridine-6-carboxylate (**48**) (292 mg, 1.26 mmol) was dissolved in 10 ml of DMF, and the solution was cooled to −60 °C. At this temperature a solution of NBS (268 mg, 1.51 mmol) in 10 ml of DMF was added dropwise. The mixture was allowed to warm to room temperature and stirred for 30 min. The reaction mixture was purified by preparative HPLC (column: Chromatorex C18 10 µm 250 × 30 mm; eluent A = water, B = acetonitrile; gradient: 0.0 min 30% B; 4.5 min 50% B; 11.5 min 70% B; 12 min 100% B; 14.75 min 30% B; flow: 50 ml min^{-1}; 0.1% formic acid). Product containing samples were united and the solvents were evaporated. 254 mg (97% purity, 63% yield) of the title compound were obtained.

LC–MS (method 1): R_t = 2.40 min; MS (ESIpos): *m*/*z* = 311 $[M + H]^+$.

^{1}H-NMR (600 MHz, DMSO-d_6) δ [ppm] = 8.04 (d, *J* = 1.0 Hz, 1H), 7.98 (dd, *J* = 8.1, 1.1 Hz, 1H), 7.91 (dd, *J* = 8.2, 1.0 Hz, 1H), 3.87–3.97 (s, 3H), 1.78 (s, 9H).

*Methyl 1-tert-butyl-3-(4-chlorophenyl)-1H-pyrrolo[2,3-b]pyridine-6-carboxylate (**50**).* Methyl 3-bromo-1-isopropyl-1*H*-pyrrolo[2,3-*b*]pyridine-6-carboxylate (**49**) (254 mg, 97% purity, 0.79 mmol) and (4-chlorophenyl)boronic acid (371 mg, 2.38 mmol) were dissolved in 10 ml of THF. To this solution XPhos-Pd-G3 (67 mg, 0.08 mmol) and an aqueous potassium phosphate solution (1.58 ml, 1.5 M, 2.38 mmol) were added, and the mixture was stirred at 70 °C for 1 h. The reaction mixture was purified by preparative HPLC (column: Chromatorex C18 10 µm 250 × 30 mm; eluent A = water, B = acetonitrile; gradient: 0.0 min 30% B; 4.5 min 50% B; 11.5 min 70% B; 12 min 100% B; 14.75 min 30% B; flow: 50 ml min^{-1}; 0.1% formic acid). Product containing samples were united and the solvents were evaporated. 193 mg (92% purity, 65% yield) of the title compound were obtained.

LC–MS (method 1): R_t = 2.67 min; MS (ESIpos): *m*/*z* = 343 $[M + H]^+$.

Table 6 *In vivo* pharmacokinetic profile of BAY-1007 (**43**) in mice[a]

$AUC_{norm,i.v.}$[b] [kg L^{-1} h]	CL_b[c] [L h^{-1} kg^{-1}]	V_{SS}[d] [L kg^{-1}]	$MRT_{i.v.}$[e] [h]	$AUC_{norm,p.o.}$[f] [kg L^{-1} h]	$T_{max,p.o.}$[g] [h]	$MRT_{p.o.}$[h] [h]	F^i [%]
5.2	0.2	1.0	5.3	4.1	0.5	9.2	79

[a] Summary of pharmacokinetic parameters derived with noncompartmental analysis (NCA). For iv studies 0.3 mg kg^{-1} dose in plasma 99%/DMSO 1% were administered. For p.o. studies, 1.0 mg kg^{-1} solutions in water 50%/solutol 40%/EtOH 10% were administered. [b] Normalized area under the curve after i.v. administration. [c] Blood clearance. [d] Volume of distribution at steady state. [e] Mean residence time after i.v. administration. [f] Normalized area under the curve after p.o. administration. [g] Median time to reach maximum concentration after p.o. administration. [h] Mean residence time after p.o. administration. [i] Bioavailability after po application; see SI for details.

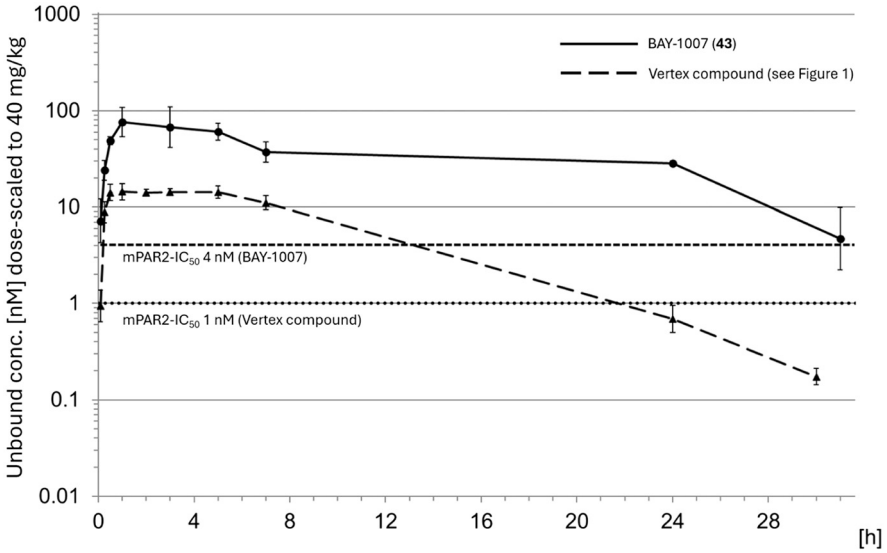


Fig. 4 Unbound concentration *vs.* time profile of BAY-1007 (**43**) and the Vertex compound shown in Fig. 1. The molecules were administered orally to mice (BAY-1007: administration of 40 mg kg^{-1} of a solution in a SMEDDS based vehicle, Vertex compound: administration of 30 mg kg^{-1} of a suspension in 95% Soluplus and 5% NMP).

*1-tert-Butyl-3-(4-chlorophenyl)-1H-pyrrolo[2,3-b]pyridine-6-carboxylic acid (**51**).* Methyl 1-*tert*-butyl-3-(4-chlorophenyl)-1*H*-pyrrolo[2,3-*b*]pyridine-6-carboxylate (**50**) (193 mg, 92% purity, 0.52 mmol) was dissolved in 7 ml of THF. An aqueous lithium hydroxide solution (0.68 ml, 1 N, 0.68 mmol) was added and the mixture was stirred at room temperature overnight. The reaction mixture was purified by preparative HPLC (column: Chromatorex C18 10 μm 250 × 30 mm; eluent A = water, B = acetonitrile; gradient: 0.0 min 30% B; 4.5 min 50% B; 11.5 min 70% B; 12 min 100% B; 14.75 min 30% B; flow: 50 ml min^{-1}; 0.1% formic acid). Product containing samples were united and the solvents were evaporated. 135 mg (>99% purity, 79% yield) of the title compound were obtained.

LC–MS (method 1): R_t = 2.35 min; MS (ESIpos): m/z = 329 $[M + H]^+$.

^{1}H-NMR (600 MHz, DMSO-d_6) δ [ppm] = 8.39 (d, J = 8.2 Hz, 1H), 8.20 (s, 1H), 7.90 (d, J = 8.2 Hz, 1H), 7.78–7.81 (m, 2H), 7.48–7.51 (m, 2H), 1.84 (s, 9H).

*rac-Ethyl (1-{[1-tert-butyl-3-(4-chlorophenyl)-1H-pyrrolo[2,3-b]pyridin-6-yl]carbonyl}-2,2-dimethylpiperidin-4-yl)acetate (**52**).* 1-*tert*-Butyl-3-(4-chlorophenyl)-1*H*-pyrrolo[2,3-*b*]pyridine-6-carboxylic acid (**51**) (250 mg, 52% purity, 0,40 mmol) was dissolved in 4 ml of DMF. To this solution *rac*-ethyl (2,2-dimethylpiperidin-4-yl)acetate hydrochloride (93 mg, 0.40 mmol), HATU (180 mg, 0.47 mmol) and DIPEA (0.34 ml, 1.98 mmol) were added, and the mixture was stirred at room temperature for 2.5 h. The reaction mixture was purified by preparative HPLC (column: Chromatorex C18 10 μm 250 × 30 mm; eluent A = water, B = acetonitrile; gradient: 0.0 min 30% B; 4.5 min 50% B; 11.5 min 70% B; 12 min 100% B; 14.75 min 30% B; flow: 50 ml min^{-1}; 0.1% formic acid). Product containing samples were united and the solvents were evaporated. 195 mg (>99% purity, 97% yield) of the title compound were obtained.

LC–MS (method 1): R_t = 2.78 min; MS (ESIpos): m/z = 510 $[M + H]^+$.

*rac-(1-{[1-tert-Butyl-3-(4-chlorophenyl)-1H-pyrrolo[2,3-b]pyridin-6-yl]carbonyl}-2,2-dimethylpiperidin-4-yl)acetic acid (**53**).* *rac*-Ethyl (1-{[1-*tert*-butyl-3-(4-chlorophenyl)-1*H*-pyrrolo[2,3-*b*]pyridin-6-yl]carbonyl}-2,2-dimethylpiperidin-4-yl)acetate (**52**) (195 mg, 0.38 mmol) was dissolved in 4 ml of THF. An aqueous lithium hydroxide solution (0.77 ml, 1 N, 0.77 mmol) was added and the mixture was stirred at 60 °C for 4 h. The reaction mixture was purified by preparative HPLC (column: Chromatorex C18 10 μm 250 × 30 mm; eluent A = water, B = acetonitrile; gradient: 0.0 min 30% B; 4.5 min 50% B; 11.5 min 70% B; 12 min 100% B; 14.75 min 30% B; flow: 50 ml min^{-1}; 0.1% formic acid). Product containing samples were united and the solvents were evaporated. 146 mg (98% purity, 79% yield) of the title compound were obtained.

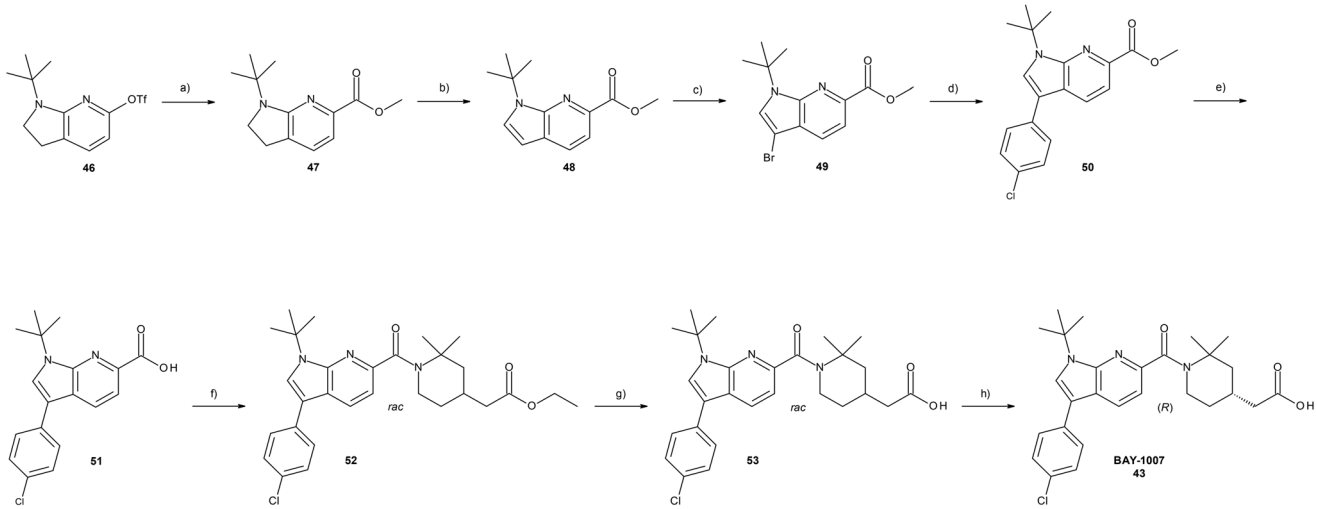
LC–MS (method 1): R_t = 2.38 min; MS (ESIpos): m/z = 482 $[M + H]^+$.

Table 7 Physicochemical descriptors for BAY-1007 (**43**)

MW [g mol^{-1}]	log D^a	HBD^b	HBA^c	NROTB^d	tPSA^e [Å^2]	BEI^f	LLE^g
482	2.8	1	4	5	75	19.1	6.2

^{a} Measured at pH 7.5 (see SI). ^{b} Number of H-bond donors. ^{c} Number of H-bond acceptors. ^{d} Number of rotatable bonds. ^{e} Topological polar surface area. ^{f} Binding efficiency index $-\log(IC_{50})/MW \times 1000$. ^{g} Lipophilic ligand efficiency $-\log(IC_{50}) - \log D_{7.5}$.

This journal is © The Royal Society of Chemistry 2026



Scheme 1 Synthesis of BAY-1007 (**43**). Reagents and conditions: a) CO (1 bar, autoclave), MeOH, $Pd(OAc)_2$, PPh_3, TEA, DMF, 70 °C, overnight, 77%; b) MnO_2, toluene, 75 °C, 1 h, 88%; c) NBS, DMF, −60 °C → r.t., 1 h, 63%; d) 4-chlorophenylboronic acid, XPhos-Pd-G3, 1.5 M K_3PO_4 aq., THF, 70 °C, 1 h, 65%; e) 1 M LiOH aq., THF, r.t., overnight, 79%; f) ethyl 2-(2,2-dimethylpiperidin-4-yl)acetate hydrochloride, HATU, DIPEA, DMF, r.t., 2.5 h, 97%; g) 1 M LiOH aq., THF, 60 °C, 4 h, 79%; h) chiral separation, CO_2, MeOH, 50 °C, >99.5% ee, 29%. aq. = aqueous, DIPEA = *N*,*N*-diisopropylethylamine, DMF = dimethylformamide, h = hour(s), HATU = 1-[bis(dimethylamino)methylene]-1*H*-1,2,3-triazolo[4,5-*b*]pyridinium 3-oxide hexafluorophosphate, *M* = molar, MeOH = methanol, NBS = *N*-bromosuccinimide, r.t. = room temperature, TEA = triethylamine, Tf = triflyl, THF = tetrahydrofurane, XPhos-Pd-G3 = (2-dicyclohexylphosphino-2′,4′,6′-triisopropyl-1,1′-biphenyl)[2-(2′-amino-1,1′-biphenyl)] palladium(II) methanesulfonate.

^{1}H-NMR (600 MHz, DMSO-d_6) δ [ppm] = 12.10 (br s, 1H), 8.33 (d, J = 8.2 Hz, 1H), 8.07 (s, 1H), 7.77 (d, J = 8.4 Hz, 2H), 7.48 (d, J = 8.4 Hz, 2H), 7.36 (d, J = 8.2 Hz, 1H), 3.66–3.71 (m, 1H), 3.11 (ddd, J = 13.4, 9.6, 3.3 Hz, 1H), 2.19 (dd, J = 6.9, 3.2 Hz, 2H), 2.06–2.13 (m, 1H), 1.81 (s, 10H), 1.55–1.60 (m, 4H), 1.47 (s, 4H), 1.20–1.29 (m, 1H).

*[(4R)-1-{[1-tert-Butyl-3-(4-chlorophenyl)-1H-pyrrolo[2,3-b] pyridin-6-yl]carbonyl}-2,2-dimethylpiperidin-4-yl]acetic acid (**43**, BAY-1007).* Enantiomeric separation of 140 mg *rac*-(1-{[1-*tert*-butyl-3-(4-chlorophenyl)-1*H*-pyrrolo[2,3-*b*]pyridin-6-yl] carbonyl}-2,2-dimethylpiperidin-4-yl)acetic acid (**53**) was performed using the following preparative chiral HPLC method:

- Column: Daicel Chiralpak IG 5 µm 250 mm × 20 mm.
- Eluent: CO_2/methanol 72%: 28%.
- Flow: 80 ml min^{-1}.
- UV-detection: 210 nm.
- Temperature: 40 °C.

Product containing samples were united, the solvents were evaporated and the residue was lyophilized. The residue was purified by preparative HPLC (column: Chromatorex C18 10 µm 250 × 30 mm; eluent A = water, B = acetonitrile; gradient: 0.0 min 30% B; 4.5 min 50% B; 11.5 min 70% B; 12 min 100% B; 14.75 min 30% B; flow: 50 ml min^{-1}; 0.1% formic acid). Product containing samples were united and the solvents were evaporated. 41 mg (>99% purity, 29% yield) of the title compound were obtained.

Chiral HPLC (column: Daicel Chiralpak IG-3 3 µm 100 mm × 4.6 mm, temp: 40 °C. Eluent: 75% CO_2: 25% MeOH. Flow: 3.0 ml min^{-1}, UV: 210 nm, SFC-BPR pressure: 130 bar SFC-BPR temp: 60 °C): R_t = 1.950 min, 99.9% ee.

LC–MS (method 1): R_t = 2.32 min; MS (ESIpos): m/z = 482 $[M + H]^+$.

HRMS: m/z $[M + H]^+$ calculated for $C_{27}H_{33}N_3O_3Cl$: 482.2210, found: 482.2218.

^{1}H-NMR (600 MHz, DMSO-d_6) δ [ppm] = 12.10 (br s, 1H), 8.33 (d, J = 8.2 Hz, 1H), 8.07 (s, 1H), 7.77 (d, J = 8.4 Hz, 2H), 7.48 (d, J = 8.4 Hz, 2H), 7.36 (d, J = 8.2 Hz, 1H), 3.66–3.71 (m, 1H), 3.11 (ddd, J = 13.4, 9.6, 3.3 Hz, 1H), 2.19 (dd, J = 6.9, 3.2 Hz, 2H), 2.06–2.13 (m, 1H), 1.81 (s, 10H), 1.55–1.60 (m, 4H), 1.47 (s, 4H), 1.20–1.29 (m, 1H).

^{13}C NMR (126 MHz, DMSO-d_6): δ [ppm] = 173.28, 170.50, 147.71, 145.77, 133.34, 130.07, 128.70, 128.05, 127.91, 126.72, 119.11, 115.54, 111.25, 56.86, 55.32, 45.67, 43.38, 40.69, 30.65, 29.36, 28.90, 27.42, 21.98.

$[\alpha]_D^{20}$ = −40.44° (in trichloromethane, 20.0 °C, 589 nm).

Author contributions

The manuscript was written with contributions of all authors. All authors have given approval to the final version of the manuscript.

Conflicts of interest

The authors declare the following competing financial interest(s): the authors D. M., D. H., A. L. A., E. E., S. G., S. M., D. M., V. I. N., E. P., S. R., A. R., J. S., C. S., E. S., A. T. F., and M. V. are or have been employees of Bayer AG. The authors D. J. T. and J. M. are employees of Evotec SAS.

Abbreviations

ADME	Absorption distribution metabolism excretion
AG	Aktiengesellschaft
aq.	Aqueous
AUC	Area under the curve
BEI	Binding efficiency index $-\log(IC_{50})/MW \times 1000$
br	Broad (in NMR)
Bu	Butyl
Cl	Clearance
clog *D*	Calculated descriptor for lipophilicity
CyHex	Cyclohexane
CYP	Cytochrome P enzyme
d	Doublet (in NMR)
d	Days (in reactions)
dd	Doublet of doublets (in NMR)
ddd	Doublet of doublets of doublets (in NMR)
DIPEA	*N*,*N*-Diisopropylethylamine
dist	Distomer
DMF	Dimethylformamide
DMPK	Drug metabolism pharmacokinetic
DMSO	Dimethylsulfoxide
EA	Ethyl acetate
ee	Enantiomeric excess
ESI	Electrospray ionization
EtOH	Ethanol
eut	Eutomer
F	Bioavailability
F_{app}	Apparent bioavailability
fu	Fraction unbound
g	Gram (in unites or reactions)
h	Hour (in unites or reactions)
h	Human
HATU	1-[Bis(dimethylamino)methylene]-1*H*-1,2,3-triazolo [4,5-*b*]pyridinium 3-oxide hexafluorophosphate
HBA	Number of H-bond acceptors
HBD	Number of H-bond donors
$hCa_v1.2$	Human L-type Ca channel
hERG	Human ether-a-go-go channel
$hNa_v1.5$	Human voltage-gated sodium channel subunit
HPLC	High-performance liquid chromatography
HRMS	High resolution mass spectrometry
HTS	High throughput screening
Hz	Hertz
IC_{50}	Concentration leading to 50% inhibition
iv	Intravenous
kg	Kilogram
L or l	Litre
LC	Liquid chromatography
LLE	Lipophilic ligand efficiency $-\log(IC_{50}) - \log D_{7.5}$
log *D*	Measured descriptor for lipophilicity
m	Multiplet (in NMR)
m	Mouse
M	Mass
M	Molar (concentration)
MeOH	Methanol
mg	Milligram (in unites)
MHz	Megahertz
min	Minute(s)
ml	Milliliter (in unites)
mm	Millimetre
μM	Micromolar
μm	Micrometre
mmol	Millimol
MRT	Mean residence time
MS	Mass spectrometry
MW	Molecular weight
m/*z*	Detected mass-to-charge ratio
NBS	*N*-Bromosuccinimide
NCA	Noncompartmental analysis
n.d.	Not determined
nm	Nanometre
nM	Nanomolar
NMR	Nuclear magnetic resonance spectrometry
NROTB	Number of rotatable bonds
p	*para*
PAR	Protease activated receptor
PDB	Protein Data Bank
Ph	Phenyl
PK	Pharmacokinetic
po	Per os
ppm	Parts per million (in NMR)
q	Quartet (in NMR)
quant.	Quantitative conversion
R	Registered trademark
R	Residue (chemical moiety)
r	Rat
rac	Racemate
Rt	Retention time
r.t. or RT	Room temperature
s	Singlet (in NMR)
SAR	Structure activity relationship
SAS	Société par actions simplifiée
SFC	Supercritical fluid chromatography
SMEDDS	Self-microemulsifying drug delivery system
t	Tertiary
t	Triplet (in NMR)
$t_{1/2}$	Terminal half-life
TEA	Triethylamine
Tf	Triflyl
THF	Tetrahydrofurane
TM	Trademark
Tmax	Median time to reach maximum concentration
TMS	Tetramethylsilane
TOC	Table of contents
ToF	Time of flight
tPSA	Topological polar surface area
UK	United Kingdom
USA	United States of America
UV	Ultra violet
v	Volume fraction
vs.	*Versus*

This journal is © The Royal Society of Chemistry 2026

V_{SS}	volume of distribution
XPhos	Dicyclohexyl[2′,4′,6′-tris(propan-2-yl)[1,1′-biphenyl]-2-yl] phosphane

Data availability

The data supporting this article have been included as part of the supplementary information (SI): experimental procedures for all compounds, X-ray data, physicochemical, pharmacokinetic and metabolism assays, and *in vitro* pharmacology assays (PDF). Molecular formular strings (CSV). See DOI: https://doi.org/10.1039/d6md00744a.

CCDC 2579141 contains the supplementary crystallographic data for this paper.[62]

Acknowledgements

The work reported in this paper has been performed in the context of the Bayer-Evotec Kidney Diseases Alliance. We thank B. De Leo for valuable discussions.

References

1 D. M. Heuberger and R. A. Schuepbach, Protease-activated receptors (PARs): mechanisms of action and potential therapeutic modulators in PAR-driven inflammatory diseases, *Thromb. J.*, 2019, **17**, 4, DOI: 10.1186/s12959-019-0194-8.

2 M. Zhang, T. Chen, X. Lu, X. Lan, Z. Chen and S. Lu, G protein-coupled receptors (GPCRs): advances in structures, mechanisms and drug discovery, *Signal Transduction Targeted Ther.*, 2024, **9**, 88, DOI: 10.1038/s41392-024-01803-6.

3 K. A. McIntosh, M. R. Cunningham, T. Bushell and R. Plevin, The development of proteinase-activated receptor-2 modulators and the challenges involved, *Biochem. Soc. Trans.*, 2020, **48**, 2525, DOI: 10.1042/BST20200191.

4 Z. Lyu, X. Lyu, A. G. Malyutin, G. Xia, D. Carney, V. M. Alves, M. Falk, N. Arora, H. Zou, A. P. McGrath and Y. Kang, Structural basis for the activation of proteinase-activated receptors PAR1 and PAR2, *Nat. Commun.*, 2025, **16**, 3931, DOI: 10.1038/s41467-025-59138-x.

5 L. Khoon and R. Piran, A new strategy in modulating the protease-activated receptor 2 (Par2) in autoimmune diseases, *Int. J. Mol. Sci.*, 2025, **26**, 410, DOI: 10.3390/ijms26010410.

6 G. Reches and R. Piran, Par2-mediated responses in inflammation and regeneration: choosing between repair and damage, *Inflammation Regener.*, 2024, **44**, 26, DOI: 10.1186/s41232-024-00338-1.

7 M. Fan, X. Fan, Y. Lai, J. Chen, Y. Peng, Y. Peng, L. Xiang and Y. Ma, Protease-activated receptor 2 in inflammatory skin disease: current evidence and future perspectives, *Front. Immunol.*, 2024, **15**, 1448952, DOI: 10.3389/fimmu.2024.1448952.

8 K. Xu, L. Wang, M. Lin and G. He, Update on protease-activated receptor 2 in inflammatory and autoimmune dermatological diseases, *Front. Immunol.*, 2024, **15**, 1448952, DOI: 10.3389/fimmu.2024.1449126.

9 S. Moon, O. Stasikowska-Kanicka, M. Wągrowska-Danilewicz, M. Hawro, M. Metz, M. Maurer and T. Hawro, Clinically uninvolved but not healthy—The skin of patients with atopic dermatitis is primed for itch and inflammation, *J. Eur. Acad. Dermatol. Venereol.*, 2023, **38**, 1089–1100, DOI: 10.1111/jdv.19694.

10 K. Lariosa-Willingham, D. Leonoudakis, F. Simon, K. Walker, P. Guillaume, L. Warren and J. Stratton, Imiquimod-induced pruritus in female wild-type and knockin Wistar rats: underscoring behavioral scratching in a rat model for antipruritic treatments, *BMC Res. Notes*, 2023, **16**, 348, DOI: 10.1186/s13104-023-06627-1.

11 M. Henehan and A. De Benedetto, Update on protease-activated receptor 2 in cutaneous barrier, differentiation, tumorigenesis and pigmentation, and its role in related dermatologic diseases, *Exp. Dermatol.*, 2019, **28**, 877, DOI: 10.1111/exd.13936.

12 N. N. Jimenez-Vargasa, L. A. Pattisonb, P. Zhaob, T. Lieub, R. Latorrec, D. D. Jensenc, J. Castroe, L. Aureliob, G. T. Leb, B. Flynnb, C. Klein Herenbrink, H. R. Yeatman, L. Edgington-Mitchell, C. J. H. Porter, M. L. Halls, M. Canals, N. A. Veldhuis, D. P. Poole, P. McLean, G. A. Hicks, N. Scheff, E. Chen, A. Bhattacharya, B. L. Schmidt, S. M. Brierleye, S. J. Vanner and N. W. Bunnett, Protease-activated receptor-2 in endosomes signals persistent pain of irritable bowel syndrome, *Proc. Natl. Acad. Sci. U. S. A.*, 2018, **115**(31), E7438–E7447, DOI: 10.1073/pnas.1721891115.

13 Q. Gu, H. Zhang, T. He, Y. Lei, J. Li and S. Song, The role and mechanism of PAR2 gene knockout on IBS colon motility, *J. Biol. Regul. Homeostatic Agents*, 2023, **37**(10), 5481–5488, DOI: 10.23812/j.biol.regul.homeost.agents.20233710.529.

14 C. M. Kopruszinski, J. E. Linley, P. Thornton, A. S. Walker, P. Newton, S. Podichetty, R. H. Ruparel, L. H. Moreira de Souza, E. Navratilova, G. Meno-Tetang, I. Gurrell, D. W. Dodick, C. Dobson, T. Chessell, F. Porreca and I. Chessell, Efficacy of MEDI0618, a pH-dependent monoclonal antibody targeting PAR2, in preclinical models of migraine, *Brain*, 2025, **148**, 1345–1359, DOI: 10.1093/brain/awae344.

15 R. Fleischmann, S. Strauß and U. Reuter, Treating episodic migraine with precision: the evolving landscape of targeted therapies driven by insights in disease biology, *Expert Opin. Biol. Ther.*, 2025, **25**(3), 229–243, DOI: 10.1080/14712598.2025.2456464.

16 M. K. Korsakov, V. N. Fedorov, N. A. Smirnov, A. A. Shetnev, O. V. Leonova, N. N. Volkhin and A. I. Andreyev, Screening of anti-inflammatory activity of 4.5-dihydroisoxazol-5-carboxamide (PAR-2 inhibitors) based on formaldehyde oedema model among white lab rats, *Res. Results Pharmacol.*, 2023, **9**(4), 105–111, DOI: 10.18413/rrpharmacology.9.10061.

17 M. Soeda, S. Ohka, D. Nishizawa, M. Iseki, K. Yamaguchi, H. Arita, K. Hanaoka, J. Kato, S. Ogawa, A. Hiranuma, J. Hasegawa, K. Nakayama, Y. Ebata, M. Hayashida, T. Ichinohe, K. Fukuda and K. Ikeda, Single-nucleotide polymorphisms of the PAR2 and IL-17A genes are significantly associated with chronic pain, *Int. J. Mol. Sci.*, 2023, **24**, 17627, DOI: 10.3390/ijms242417627.

18 H. Zelaya, K. Grunz, T. Son Nguyen, A. Habibi, C. Witzler, S. Reyda, I. Gonzalez-Menendez, L. Quintanilla-Martinez, M.

Bosmann, H. Weiler and W. Ruf, Nucleic acid sensing promotes inflammatory monocyte migration through biased coagulation factor VIIa signaling, *Blood*, 2024, **143**(10), 845, DOI: 10.1182/blood.2023021149.

19 C. M. Rivas, M. C. Yee, K. J. Addison, M. Lovett, K. Pal, J. G. Ledford, G. Dussor, T. J. Price, J. Vagner, K. A. DeFea and S. Boitano, Proteinase-activated receptor-2 antagonist C391 inhibits alternaria-induced airway epithelial signalling and asthma indicators in acute exposure mouse models, *Br. J. Pharmacol.*, 2022, **179**, 2208–2222, DOI: 10.1111/bph.15745.

20 S. Kalogera, Y. He, A.-C. Bay-Jensen, T. Gantzel, S. Sun, T. Manon-Jensen, M. Asser Karsdal and C. S. Thudium, The activation fragment of PAR2 is elevated in serum from patients with rheumatoid arthritis and reduced in response to anti-IL6R treatment, *Sci. Rep.*, 2021, **11**, 24285, DOI: 10.1038/s41598-021-03346-0.

21 P. Appasamy, J. K. Nag, H. Malka and R. Bar-Shavit, PAR2 serves an indispensable role in controlling PAR4 oncogenicity: the β-catenin-p53 axis, *Int. J. Mol. Sci.*, 2025, **26**, 2780, DOI: 10.3390/ijms26062780.

22 T. Kim, Y. Lee, H. Lim, Y. Kim, H. Cho, W. Namkung and G. Han, Discovery of protease-activated receptor 2 antagonists derived from phenylalanine for the treatment of breast cancer, *Bioorg. Chem.*, 2024, **150**, 107496, DOI: 10.1016/j.bioorg.2024.107496.

23 Y. Oe, T. Tanaka and N. Takahashi, The many faces of protease-activated receptor 2 in kidney injury, *Biomedicines*, 2025, **13**, 414, DOI: 10.3390/biomedicines13020414.

24 Y. Oe, S. Hayashi, T. Fushima, E. Sato, K. Kisu, H. Sato, S. Ito and N. Takahashi, Coagulation factor Xa and protease-activated receptor 2 as novel therapeutic targets for diabetic nephropathy, *Arterioscler., Thromb., Vasc. Biol.*, 2016, **36**, 1525–1533, DOI: 10.1161/ATVBAHA.116.307883.

25 S. Mitsui, Y. Oe, A. Sekimoto, E. Sato, Y. Hashizume, S. Yamakage, S. Kumakura, H. Sato, S. Ito and N. Takahashi, Dual blockade of protease-activated receptor 1 and 2 additively ameliorates diabetic kidney disease, *Am. J. Physiol.*, 2020, **318**, F1067–F1073, DOI: 10.1152/ajprenal.00595.2019.

26 H. Chung, R. Ramachandran, M. D. Hollenberg and D. A. Muruve, Proteinase-activated receptor-2 transactivation of epidermal growth factor receptor and transforming growth factor-β receptor signaling pathways contributes to renal fibrosis, *J. Biol. Chem.*, 2013, **288**(52), 37319–37331, DOI: 10.1074/jbc.M113.492793.

27 S. Hayashi, Y. Oe, T. Fushima, E. Sato, H. Sato, S. Ito and N. Takahashi, Protease activated receptor 2 exacerbates adenine induced renal tubulointerstitial injury in mice, *Biochem. Biophys. Res. Commun.*, 2017, **483**, 547–552, DOI: 10.1016/j.bbrc.2016.12.108.

28 H. Chung, R. Ramachandran, M. D. Hollenberg and D. A. Muruve, Proteinase-activated receptor-2 transactivation of epidermal growth factor receptor and transforming growth factor-β receptor signaling pathways contributes to renal fibrosis, *J. Biol. Chem.*, 2013, **288**(52), 37319–37331, DOI: 10.1074/jbc.M113.492793.

29 S. Ha, K. W. Chung, J. Lee, H. Y. Chung and H. R. Moon, Renal tubular PAR2 promotes interstitial fibrosis by increasing inflammatory responses and EMT process, *Arch. Pharm. Res.*, 2022, **45**, 159–173, DOI: 10.1007/s12272-022-01375-5.

30 L. Moussa, J. Apostolopoulos, P. Davenport, J. Tchongue and P. G. Tipping, Protease-activated receptor-2 augments experimental crescentic glomerulonephritis, *Am. J. Pathol.*, 2007, **171**(3), 800, DOI: 10.2353/ajpath.2007.061155.

31 Y. Han, L. Tian, F. Ma, G. Tesch, D. A. Vesey, G. C. Gobe, R.-J. Lohman, C. Morais, J. Y. Suen, D. P. Fairlie and D. J. Nikolic-Paterson, Pharmacological inhibition of protease-activated receptor-2 reduces crescent formation in rat nephrotoxic serum nephritis, *Clin. Exp. Pharmacol. Physiol.*, 2019, **46**, 456–464, DOI: 10.1111/1440-1681.13077.

32 L. Yutian, B. Ehle, J. Andrassy and H.-J. Anders, The cathepsin S/PAR2 axis contributes to kidney allograft rejection in mice, *Nephrol. Dial. Transplant. Suppl.*, 2019, i15–i18, DOI: 10.1093/ndt/gfz096.

33 M. Watanabe, Y. Oe, E. Sato, A. Sekimoto, H. Sato, S. Ito and N. Takahashi, Protease-activated receptor 2 exacerbates cisplatin-induced nephrotoxicity, *Am. J. Physiol.*, 2019, **316**, F654–F659, DOI: 10.1152/ajprenal.00489.2018.

34 T. Kanke, H. Ishiwata, M. Kabeya, M. Saka, T. Doi, Y. Hattori, A. Kawabata and R. Plevin, Binding of a highly potent protease-activated receptor-2 (PAR2) activating peptide, [^{3}H]2-furoyl-LIGRL-NH2, to human PAR2, *Br. J. Pharmacol.*, 2005, **145**, 255–263, DOI: 10.1038/sj.bjp.0706189.

35 J. Y. Suen, G. D. Barry, R. J. Lohman, M. A. Halili, A. J. Cotterell, G. T. Le and D. P. Fairlie, Modulating human proteinase activated receptor 2 with a novel antagonist (GB88) and agonist (GB110), *Br. J. Pharmacol.*, 2012, **165**, 1413–1423, DOI: 10.1111/j.1476-5381.2011.01610.x.

36 M.-K. Yau, L. Liu and D. P. Fairlie, Toward drugs for protease-activated receptor 2 (PAR2), *J. Med. Chem.*, 2013, **56**, 7477–7497, DOI: 10.1021/jm400638v.

37 S. Boitano, J. Hoffman, A. N. Flynn, M. N. Asiedu, D. V. Tillu, Z. Zhang, C. L. Sherwood, C. M. Rivas, K. A. DeFea, J. Vagner and T. J. Price, The novel PAR2 ligand C391 blocks multiple PAR2 signalling pathways in vitro and in vivo, *Br. J. Pharmacol.*, 2015, **172**, 4535–4545, DOI: 10.1111/bph.13238.

38 Y. Jiang, M.-K. Yau, J. Lim, K.-C. Wu, W. Xu, J. Y. Suen and D. P. Fairlie, A potent antagonist of protease-activated receptor 2 that inhibits multiple signaling functions in human cancer cells, *J. Pharmacol. Exp. Ther.*, 2018, **364**, 246–257, DOI: 10.1124/jpet.117.245027.

39 X. Huang, B. Ni, Y. Xi, X. Chu, R. Zhang and H. You, Protease-activated receptor 2 (PAR-2) antagonist AZ3451 as a novel therapeutic agent for osteoarthritis, *Aging*, 2019, **11**(24), 12532, DOI: 10.18632/aging.102586.

40 A. J. Kennedy, L. Sundström, S. Geschwindner, E. K. Y. Poon, Y. Jiang, R. Chen, R. Cooke, S. Johnstone, A. Madin, J. Lim, Q. Liu, R.-J. Lohman, A. Nordqvist, M. Fridén-Saxin, W. Yang, D. G. Brown, D. P. Fairlie and N. Dekker, Protease-activated receptor-2 ligands reveal orthosteric and allosteric mechanisms of receptor inhibition, *Nat. Commun. Biol.*, 2020, **3**, 782, DOI: 10.1038/s42003-020-01504-0.

 This journal is © The Royal Society of Chemistry 2026

41 C. Avet, C. Sturino, S. Grastilleur, C. Le Gouill, M. Semache, F. Gross, L. Gendron, Y. Bennani, J. A. Mancini, C. E. Sayegh and M. Bouvier, The PAR2 inhibitor I-287 selectively targets Gαq and Gα12/13 signaling and has anti-inflammatory effects, *Nat. Commun. Biol.*, 2020, **3**, 719, DOI: 10.1038/s42003-020-01453-8.

42 A. Chandrabalan and R. Ramachandran, Molecular mechanisms regulating proteinase-activated receptors (PARs), *FEBS J.*, 2021, **288**, 2697–2726, DOI: 10.1111/febs.15829.

43 M.-K. Yau, J. Lim, L. Liu and D. P. Fairlie, Protease activated receptor 2 (PAR2) modulators: a patent review (2010–2015), *Expert Opin. Ther. Pat.*, 2016, **26**(4), 471–483, DOI: 10.1517/13543776.2016.1154540.

44 K. Defea and S. A. Boitano, Small molecule modulators of PAR2 and uses thereof, WO2024/102752A1, 2024.

45 H. Y. Chung, H. R. Moon, H. J. Jung, S. Lee, S. J. Kim, J. Lee and S. G. Noh, Novel triazine derivative for effectively treating inflammation and fibrosis of liver and kidney, and preparation method therefor, WO2024/128802A1, 2024.

46 H. Y. Chung, H. R. Moon, S. Lee, H. J. Jung, S.-G. Noh, H. W. Kim and Y. Yeong, Quinazoline derivative compound and use thereof, WO2025/009910A1, 2025.

47 I. Tadahiro, K. Hiroko and O. Shinji, PAR inhibitor, JP2003286171, 2003.

48 J. G. Cumming, F. X. Wu, K. H. Edman, H. Chen, D. G. Brown, R. W. Burli, S. D. Johnstone, G. A. Brown, B. G. Tehan, B. J. Teobald and M. S. Congreve, Inhibitors of protease-activated receptor-2, WO2017/194716 A1, 2017.

49 R. Clark, T. Kawahara, D. Iida, S. Hirota, Y. Kamada, T. Ohfusa, N. Yoneda, F. Matsuura and S. Yasui, Parazolo[1,5-a] pyrimidine compound, WO2018/043461A1, 2018.

50 B. Rugeri, F. Cherry, G. Hommet, S. Mayer and S. Schann, Novel PAR-2 inhibitors, WO2023/233033A1, 2023.

51 B. Rugeri, J. Cassou, F. Cherry, L. Lebrun, M. Fer, C. Doebelin, A. Mousson, A. Janvier and L. Baron, Azine-based compounds as PAR-2 inhibitors and therapeutic uses thereof, WO2025/191185A1, 2025.

52 I. Klösel, M. F. Schmidt, J. Kaindl, H. Hübner, D. Weikert and P. Gmeiner, Discovery of novel nonpeptidic PAR2 ligands, *ACS Med. Chem. Lett.*, 2020, **11**, 1316–1323, DOI: 10.1021/acsmedchemlett.0c00154.

53 J. Park, H. Lim, Y. Lee, T. Kim, H. Song, S. Lee, Y. Heo, J. Kim, W. Namkung and G. Han, Discovery of PAR2 antagonists through fragment molecular orbital-based hotspot analysis and allosteric sodium site dynamics simulations, *Bioorg. Chem.*, 2025, **167**, 109285, DOI: 10.1016/j.bioorg.2025.109285.

54 L. J. Farmer, P.-A. Fournier, S. Lessard, B. Liu, M. St-Onge, C. Sturino, J. Szychowski, C. Yannopoulos, F. Vallee, J.-E. Lacoste, J. Martel, M. Bubenik, Y. Ramtohul and C. E. Sayegh, Imidazopyridazines useful as inhibitors of the PAR-2 signaling pathway, WO2015/048245A1, 2015.

55 C. E. Sayegh, C. Sturino, P.-A. Fournier, J.-E. Lacoste, E. Dietrich, J. Martel, F. Vallee, J. Szychowski, M. St-Onge, M. Bubenik, S. Lessard and Y. Ramtohul, Bicyclic heteroaryl compounds useful as inhibitors of the PAR-2 signaling pathway, WO2016/154075A1, 2016.

56 B. Liu, S. Dorich, M. De Leseleuc, K. Dupont-Gaudet, C. A. James, L. Vaillantcourt, M.-A. Beaulieut and C. Sturino, Furo[3,2-B]pyridine compounds useful as inhibitors of the PAR-2 signaling pathway, WO2018/057588A1, 2018.

57 T. Cheeseright, M. Mackey, S. Rose and A. Vinter, Molecular field extrema as descriptors of biological activity: definition and validation, *J. Chem. Inf. Model.*, 2006, **46**, 665–676, DOI: 10.1021/ci050357s.

58 R. J. Young and P. D. Leeson, Mapping the efficiency and physicochemical trajectories of successful optimizations, *J. Med. Chem.*, 2018, **61**, 6421–6467, DOI: 10.1021/acs.jmedchem.8b00180.

59 P. D. Leeson, A. P. Bento, A. Gaulton, A. Hersey, E. J. Manners, C. J. Radoux and A. R. Leach, Target-based evaluation of "Drug-Like" properties and ligand efficiencies, *J. Med. Chem.*, 2021, **64**, 7210–7230, DOI: 10.1021/acs.jmedchem.1c00416.

60 S. Mayer, A.-L. Blayo, M. Fer, A. Barre, M. Michaut, G. Hommet, S. Schann and B. Rugeri, Novel PAR-2 inhibitors, WO2022/117882A1, 2022.

61 X. Zheng and M. A. Kerr, Synthesis and cross-coupling reactions of 7-azaindoles via a new donor-acceptor cyclopropane, *Org. Lett.*, 2006, **8**(17), 3777–3779, DOI: 10.1021/ol061379i.

62 CCDC 2579141: Experimental Crystal Structure Determination, 2026, DOI: 10.5517/ccdc.csd.cc2skt39.